

Control of the corner separation in a compressor cascade by steady and unsteady plasma aerodynamic actuation

Ying-hong Li · Yun Wu · Min Zhou · Chang-bing Su · Xiong-wei Zhang · Jun-qiang Zhu

Received: 21 October 2008 / Revised: 5 November 2009 / Accepted: 5 November 2009 / Published online: 26 November 2009
© Springer-Verlag 2009

Abstract This paper reports experimental results on using steady and unsteady plasma aerodynamic actuation to control the corner separation, which forms over the suction surface and end wall corner of a compressor cascade blade passage. Total pressure recovery coefficient distribution was adopted to evaluate the corner separation. Corner separation causes significant total pressure loss even when the angle of attack is 0° . Both steady and unsteady plasma aerodynamic actuations suppress the corner separation effectively. The control effect obtained by the electrode pair at 25% chord length is as effective as that obtained by all four electrode pairs. Increasing the applied voltage improves the control effect while it augments the power requirement. Increasing the Reynolds number or the angle of attack makes the corner separation more difficult to control. The unsteady actuation is much more effective and requires less power due to the coupling between the unsteady actuation and the separated flow. Duty cycle and excitation frequency are key parameters in unsteady plasma flow control. There are thresholds in both the duty cycle and the excitation frequency, above which the control effect saturates. The maximum relative reduction in total pressure loss coefficient achieved is up to 28% at 70% blade span. The obvious difference between steady and unsteady actuation may be that wall jet governs the flow control effect of steady actuation, while much more

vortex induced by unsteady actuation is the reason for better control effect.

List of symbols

c	Chord length
t	Blade spacing
h	Blade height
β_1	Inlet-air angle
β_2	Outlet-air angle
β_s	Blade stagger angle
i	Angle of attack
v_∞	Freestream velocity
Re	Reynolds number based on the axial chord length and the freestream velocity
T_1	Static temperature at the cascade inlet
P_1	Static pressure at the cascade inlet
P_1^*	Total pressure at the cascade inlet
P_2	Static pressure at the cascade outlet
P_2^*	Total pressure at the cascade outlet
σ	Total pressure recovery coefficient
ω	Total pressure loss coefficient
ω_{baseline}	Total pressure loss coefficient without actuation
ω_{actuated}	Total pressure loss coefficient with actuation
$\delta(\omega)$	Relative reduction in the total pressure loss coefficient
$\delta(\omega)_{\text{max}}$	Relative reduction in the maximum total pressure loss coefficient
d_1	Upper electrode width
d_2	Lower electrode width
Δd	Inner space of an electrode pair
h_e	Electrode height
h_d	Dielectric layer height
D	Space between adjacent electrode pairs
T_{ac}	Period of the steady plasma aerodynamic actuation

Y. Li · Y. Wu (✉) · M. Zhou · C. Su · X. Zhang
Engineering College, Air Force Engineering University,
Xi'an, China
e-mail: wuyun1223@126.com

J. Zhu
Institute of Engineering Thermophysics,
Chinese Academy of Sciences, Beijing, China

F	Driving frequency of the high voltage sine wave
T_{signal}	Period of the unsteady plasma aerodynamic actuation on duty
T_{control}	Period of the unsteady plasma aerodynamic actuation
f	Excitation frequency of the unsteady plasma aerodynamic actuation
α	Duty cycle of the unsteady plasma aerodynamic actuation
C	Characteristic length of the axial separation region at the endwall
S_r	Strouhal number based on the characteristic length and the local freestream velocity

1 Introduction

Higher total pressure ratio, higher efficiency, less stage number and larger stable operating range are main characteristics of the future aero-engine compressor. Flow separation is the ultimate reason for the compressor stability and efficiency reduction. Corner separation, which forms over the suction surface and the endwall corner of the blade passage, appears to be universal for the corners of both stator and rotor blades without tip clearance (Dong et al. 1987; Place 1997). Deleterious consequences of the corner separation mainly include passage blockage and considerable total pressure loss, which lead to reduction in the compressor performance (Place 1997). Thus, control of the corner separation is one of the important ways of improving axial compressor stability and efficiency. In addition, from a compressor design standpoint, less number of more highly loaded stages is desirable to minimize compressor cost, weight and length. Therefore, active separation control provides the best opportunity to achieve an overall improvement in the compressor performance.

Systemic studies on how to describe, predict and control the corner separation have been carried out (Dong et al. 1987; Place 1997; Gbadebo 2003; Gbadebo et al. 2005; Gbadebo et al. 2008). Three dimensional computational fluid dynamics, based on a linear treatment of the Navier–Stokes equations, can predict properties of the corner separation (Gbadebo et al. 2005). An appropriately applied boundary layer suction of up to 0.7% of inlet mass flow can control and eliminate typical compressor stator hub corner separation over a range of angle of attack, which is confirmed by increased blade loading, enhanced average static pressure rise, significant loss removal, and a uniform exit flow in computations and experiments (Gbadebo et al. 2008). Vortex generator, which produces a strong vortex in order to enhance the mixing between the main flow and the

retarded boundary layer at the side wall, can control and reduce corner separation effectively (Hergt et al. 2006).

Our approach to control the corner separation is based on the use of plasma aerodynamic actuation, which is promising in improving aircraft aerodynamic characteristics and propulsion efficiency (Moreau 2007; Corke et al. 2007). A plasma aerodynamic actuator, which consists of electrode pairs separated by a thin dielectric insulator, has the merits of robustness, simplicity, low power consumption and real-time control at high frequency. The plasma aerodynamic actuation has drawn considerable attention and has been used in airfoil leading edge separation control (Roth and Sherman 2000; Corke et al. 2007; Benard et al. 2008; Benard et al. 2009), bluff body flow separation control (Sung et al. 2006), axial compressor stability extension (Wu et al. 2007), high speed jet control (Samimy et al. 2007), transition delay (Grundmann and Tropea 2007) and so on. However, little attention has been drawn to the use of plasma aerodynamic actuation in the corner separation control of axial compressors.

The object of our research is to use plasma aerodynamic actuation to control the corner separation in a compressor cascade, so as to minimize total pressure loss caused by entropy increase due to mixing of nonuniform separated flow with main flow.

2 Experimental setup

2.1 Cascade facility and experimental procedure

Experiments were carried out on a low-speed compressor cascade facility, as shown in Fig. 1. The total inlet conditions are held constant by a pneumatic butterfly valve controlled via a personal computer. The incoming flow is straightened and passes through a series of wire-mesh grids

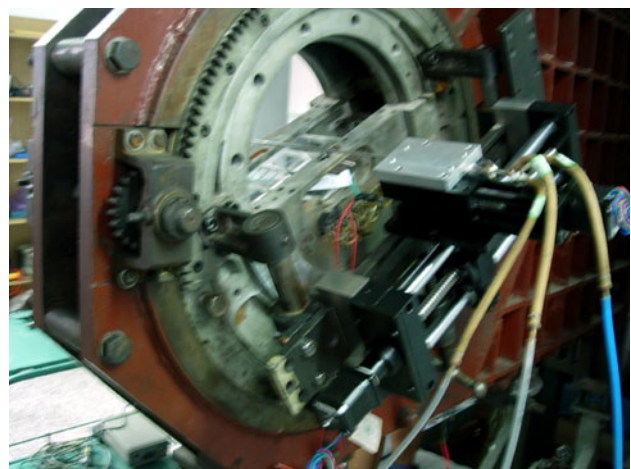


Fig. 1 The low-speed compressor cascade facility

to generate a uniform flow field at the test section inlet. A nozzle upstream of the test section accelerates the flow as it enters inside the cascade. Downstream of the test section, the flow exits through an exhaust duct and a muffler venting to the atmospheric conditions outside of the testing facility. The freestream turbulence ranges from 0.4 to 0.6%. The endwall boundary layer is laminar, and the thickness is about 8 mm, 8% of the blade span.

The low-speed compressor cascade, which consists of seven blades made of organic glass, was used in this study. The cascade can be rotated to adjust the inlet flow angle. Main cascade parameters are shown in Fig. 2. Only the middle blade was laid with the plasma aerodynamic actuator.

Total pressure distributions at 10 mm, which is 15% of the chord length, downstream of the blade trailing edge along the pitch direction at 50, 60 and 70% blade spans were measured with and without the plasma aerodynamic actuation. A three-hole probe calibrated for pitch, and yaw was used to measure the total pressure at the cascade exit. The uncertainty of the pressure measurements was calculated to be about 1% of the measured pressure in which the digital quantization and calibration errors were included.

Two parameters, total pressure recovery coefficient σ and the relative reduction in the total pressure loss coefficient $\delta(\omega)$, were used to quantify the performance improvement due to the plasma aerodynamic actuation.

The total pressure recovery coefficient σ for a blade passage is defined as

$$\sigma = P_2^*/P_1^* \tag{1}$$

The relative reduction in the total pressure loss $\delta(\omega)$ for a blade passage is defined as

$$\omega = (P_1^* - P_2^*) / (P_1^* - P_1) \tag{2}$$

$$\delta(\omega) = (\omega_{\text{baseline}} - \omega_{\text{actuated}}) / \omega_{\text{baseline}} \times 100\% \tag{3}$$

Here, P_1, P_1^*, P_2 and P_2^* are static pressure at the cascade inlet, total pressure at the cascade inlet, static pressure at the cascade exit and total pressure at the cascade exit, respectively.

2.2 Plasma aerodynamic actuator

A schematic of an asymmetric surface dielectric barrier discharge plasma aerodynamic actuator is shown in Fig. 3. The dielectric layer is a Teflon plate with a relative permittivity constant of 2.2. The electrodes are made of copper. An ac input high voltage is supplied on the electrodes. When the ac amplitude is large enough, the air is weakly ionized in the region of the largest electric potential. Coulomb force acting on the charged species (Moreau 2007; Corke et al. 2007; Boeuf et al. 2007) resulting in momentum transfer between ions and neutral molecules. Then, an electric wind of several m/s is produced. This electric wind velocity depends strongly on the electrical and geometrical parameters of the plasma aerodynamic actuator (Moreau 2007; Forte et al. 2007).

The plasma aerodynamic actuator used in the present experiments consists of four electrode pairs, located at 5, 25, 50 and 75% of the chord length, respectively. The electrode pair at 5% of chord length is named as the 1st electrode pair. A sketch of a blade with the actuator on the surface is shown in Fig. 4. The electrode thickness is not to scale in the figure. The electrodes are parallel to the leading edge of the blade. The wall jet induced by the plasma aerodynamic actuation is locally parallel to the blade surface.

The plasma aerodynamic actuator is driven by a high frequency high voltage power supply (CTP-2000 M+, Suman Electronics). The output waveform is sinewave. The output ranges of the peak-to-peak voltage and the driving frequency of the power supply are $V_{p-p} = 0\text{--}40$ kV

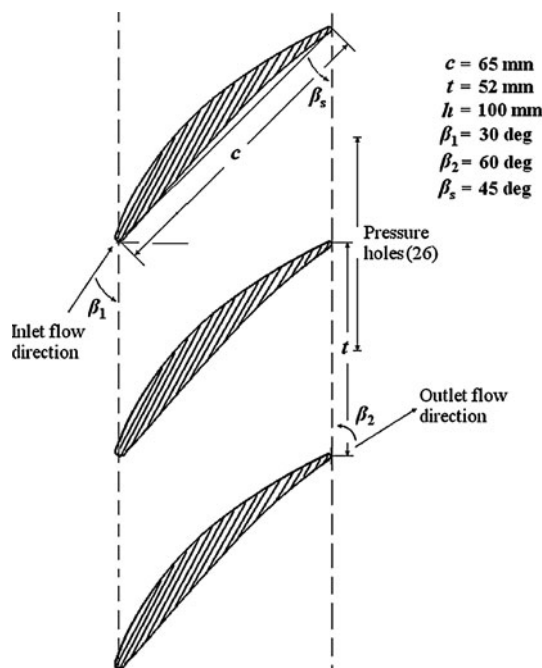


Fig. 2 Compressor cascade parameters

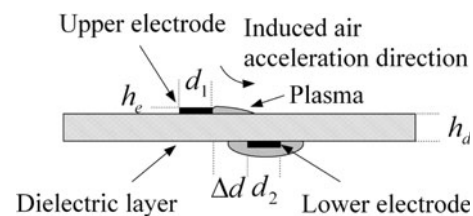


Fig. 3 A schematic of the asymmetric surface dielectric barrier discharge plasma aerodynamic actuator. $d_1 = 2$ mm, $d_2 = 2$ mm, $\Delta d = 1$ mm, $h_d = 0.5$ mm and $h_c = 0.035$ mm, respectively. The electrode length is 100 mm

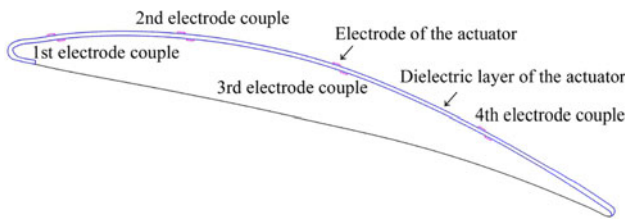


Fig. 4 A sketch of a blade with plasma aerodynamic actuator

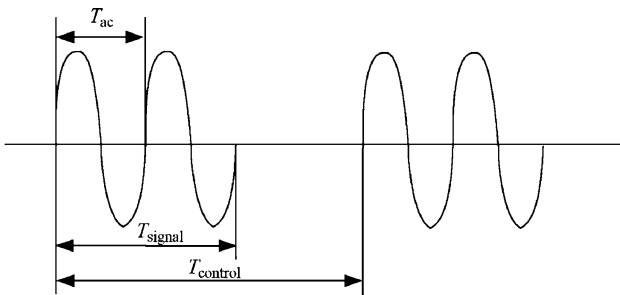


Fig. 5 The signal sent to the plasma aerodynamic actuator during unsteady excitation

and $F = 6\text{--}40$ kHz, respectively. The driving frequency is fixed at 23 kHz in the experiments.

The plasma aerodynamic actuator works at steady or unsteady mode in the experiments. In the steady mode, the actuator is operated at the ac frequency. In the unsteady mode of operation, the ac voltage is cycled off and on. Figure 5 shows a typical signal sent to the plasma aerodynamic actuator during the unsteady actuation, which is similar to that used by other groups (Corke et al. 2007).

Two important parameters of the unsteady plasma aerodynamic actuation are the excitation frequency f , and the duty cycle α defined in Eqs. 4 and 5, respectively.

$$f = 1/T_{\text{control}} \tag{4}$$

$$\alpha = T_{\text{signal}}/T_{\text{control}} \times 100\% \tag{5}$$

The output ranges of the excitation frequency and the duty cycle are $f = 100\text{--}1,000$ Hz and $\alpha = 5\text{--}90\%$, respectively.

The applied voltage and the total discharge current were monitored by a voltage probe (Tektronix P6015A) and a current probe (Tektronix P6022), respectively. The two signals were recorded by a two-channel digital oscilloscope (Tektronix TDS3012B). The uncertainty of the measurements was calculated to be about 1.3% of the measured value.

3 Results and discussion

3.1 Baseline conditions

The objective of the measurements is to document the effect of the corner separation on the total pressure loss of

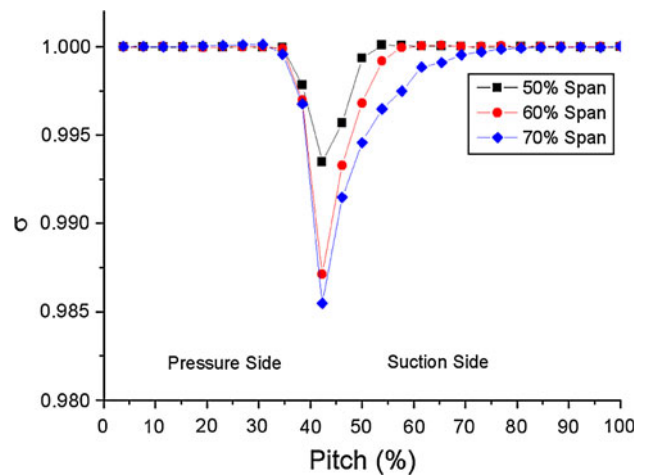


Fig. 6 Total pressure recovery coefficient distributions along the pitch direction at different blade spans ($v_\infty = 50$ m/s, $i = 0^\circ$)

the blade. The freestream velocity, inlet static temperature and outlet static pressure are $v_\infty = 50$ m/s (corresponding Re is 223,000), $T_1 = 293$ K and $P_2 = 101,545$ Pa, respectively. When the angle of attack is $i = 0^\circ$, total pressure recovery coefficient distributions at cascade exit along the pitch direction at different blade spans are measured, as shown in Fig. 6. The wake width covers 19, 23 and 42% blade pitch at 50, 60 and 70% blade span, respectively. There is almost no flow separation at the mid-span. Due to the corner separation, the total pressure loss at 60 and 70% blade span is much higher than that at the mid-span.

When the angle of attack increases to 2 and 4°, the corner separation becomes much more serious, as shown in Fig. 7. Thus, it can be concluded that the corner separation is an important flow phenomenon at small angle of attack or even 0° for the compressor cascade in our experiments. The separations contribute greatly to passage blockage, which effectively places a limit on the loading and static

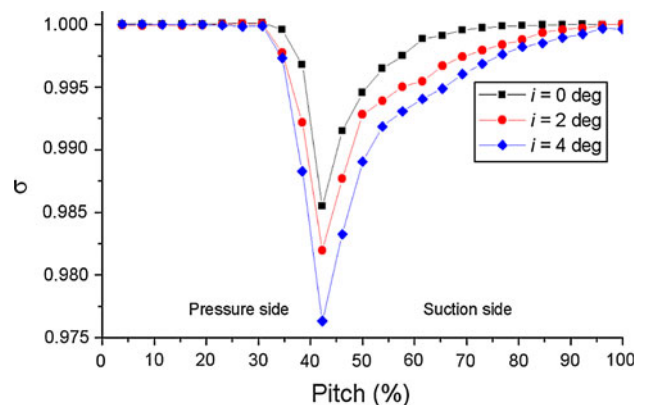


Fig. 7 Total pressure recovery coefficient distributions at different angles of attack ($v_\infty = 50$ m/s, 70% Span)

pressure rise achievable by the compressor (Gbadebo et al. 2005).

3.2 Steady plasma flow control experiment results

Total pressure recovery coefficient distributions along the pitch direction with and without steady plasma aerodynamic actuation are shown in Figs. 8, 9 and 10. The angle of attack is $i = 0^\circ$. All four electrode pairs are switched on. The waveform is continuous sine wave. The applied peak-to-peak voltage and driving frequency are $V_{p-p} = 10$ kV and $F = 23$ kHz, respectively.

The total pressure recovery coefficient at 50% blade span remains almost unchanged while $\delta(\omega)_{\max}$ at 60 and 70% blade span are 13.8 and 10.7%, respectively, with steady plasma aerodynamic actuation. The mechanism of

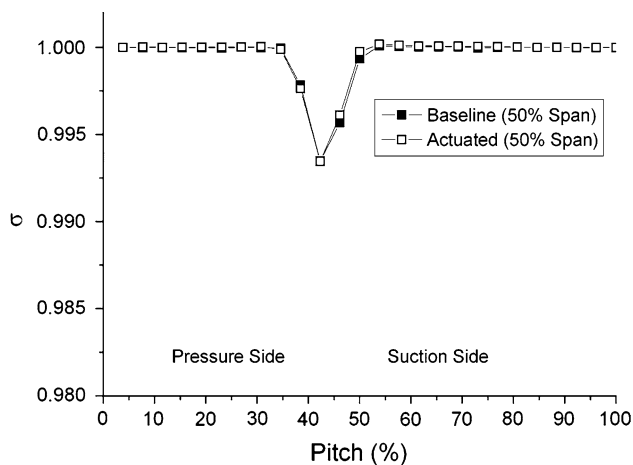


Fig. 8 Total pressure recovery coefficient distributions with and without steady plasma aerodynamic actuation at 50% blade span ($v_\infty = 50$ m/s, $i = 0^\circ$, $V_{p-p} = 10$ kV, $F = 23$ kHz)

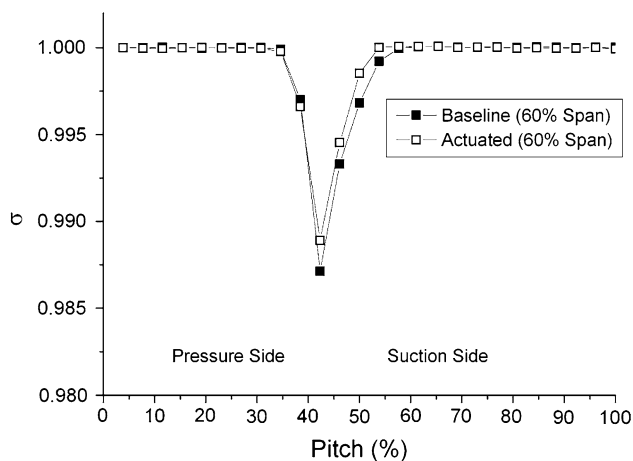


Fig. 9 Total pressure recovery coefficient distributions with and without steady plasma aerodynamic actuation at 60% blade span ($v_\infty = 50$ m/s, $i = 0^\circ$, $V_{p-p} = 10$ kV, $F = 23$ kHz)

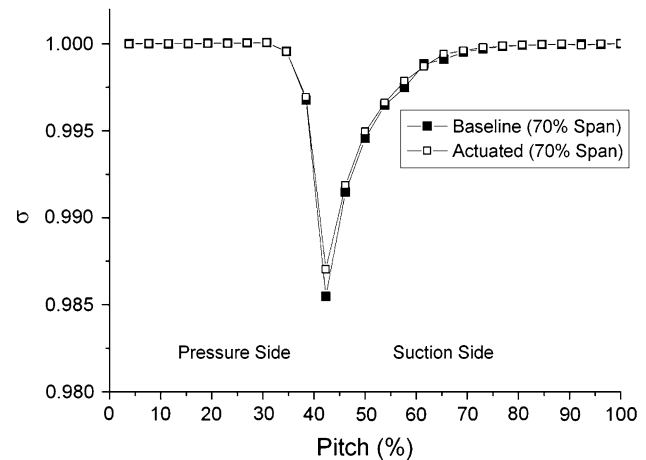


Fig. 10 Total pressure recovery coefficient distributions with and without steady plasma aerodynamic actuation at 70% blade span ($v_\infty = 50$ m/s, $i = 0^\circ$, $V_{p-p} = 10$ kV, $F = 23$ kHz)

steady plasma aerodynamic actuation to control the corner separation may be that the actuation induces a time-averaged body force on the flow as a result of the flow that cannot respond to such high frequency (23 kHz in the experiments) disturbances. A wall jet, which is oriented in the mean flow direction, is produced to add momentum to the near-wall boundary layer near the flow separation location. The energized flow is able to withstand the adverse pressure gradient without separation. The directed wall jet governs the flow control effect of steady plasma aerodynamic actuation. The power consumed by the plasma aerodynamic actuator was calculated using the measured voltage and discharge current (Falkenstein and Coogan 1997; Borcia et al. 2003; Nersisyan and Graham 2004). The power dissipated by all four electrode pairs is 37.9 W. The length of each electrode pair is 100 mm. When the electrode length is enlarged, the consumed power increases nonlinearly.

3.2.1 Effect of the actuation location

The location of the plasma aerodynamic actuation is a key parameter in plasma flow control experiments. Total pressure recovery coefficients with steady actuation at different locations are shown in Fig. 11. The applied peak-to-peak voltage and driving frequency are $V_{p-p} = 10$ kV and $F = 23$ kHz, respectively.

$\delta(\omega)_{\max}$ is 5.5, 10.3, 2.4 and 0.07% when the 1st, 2nd, 3rd and 4th electrode pair is switched on, respectively. The 2nd electrode pair at 25% chord length is the most effective, and the control effect is as the same as that obtained by all four electrode pairs. The power dissipated by the 2nd electrode pair is just 18.4 W, about half of the power dissipated by all four electrode pairs. Therefore, the actuation location is vital to the control effect in corner separation

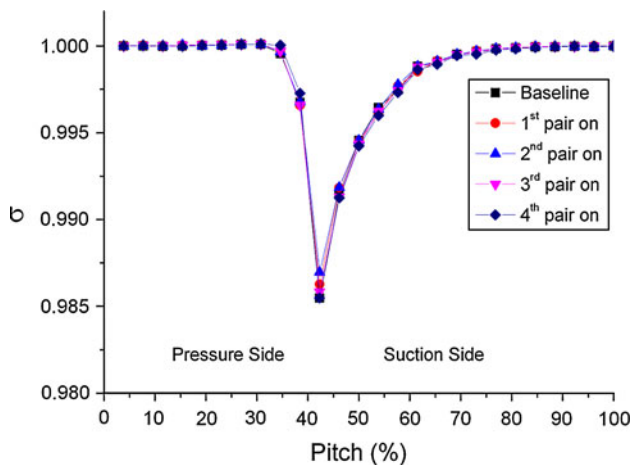


Fig. 11 Total pressure recovery coefficients with steady actuation at different locations ($v_\infty = 50$ m/s, $i = 0^\circ$, $V_{p-p} = 10$ kV, $F = 23$ kHz, 70% Span)

control. In separation control of low-pressure turbine blades (Huang et al. 2006), the optimum chordwise placement for the plasma aerodynamic actuator is just upstream of the flow separation location. In the flow separation control above a NACA 0015 airfoil (Jolibois et al. 2008), plasma aerodynamic actuation at the separation point is more effective, and the actuator placed just upstream or at the separation point requires the minimum electrical power consumption. In corner separation control by tailored boundary layer suction (Gbadebo et al. 2008), the optimum slot should be long enough to be sure to remove the limiting streamline, and the suction upstream of the corner separation location at the suction surface is most important for the control effect. Therefore, it can be inferred that the location of the 2nd electrode pair is just upstream of the corner separation.

3.2.2 Effect of the actuation strength

The plasma aerodynamic actuation strength is another important parameter in plasma flow control experiments. The body force increases with the voltage amplitude in proportion to the volume of plasma (ionized air) and the strength of the electric field gradient (Huang et al. 2006). As the applied peak-to-peak voltage increases from 8 to 12 kV, $\delta(\omega)_{\max}$ increases from 2.7 to 11.1%, as shown in Fig. 12.

The 2nd electrode pair at 25% chord length is switched on, and the driving frequency is 23 kHz. The power dissipation increases from 8.4 to 23.5 W when the applied peak-to-peak voltage increases from 8 to 12 kV. When the applied voltage is less than 9 kV, the control effect is very tiny. When the applied voltage is higher than 10 kV, the control effect saturates, and further increases in the voltage amplitude show no evident benefit, which is similar with

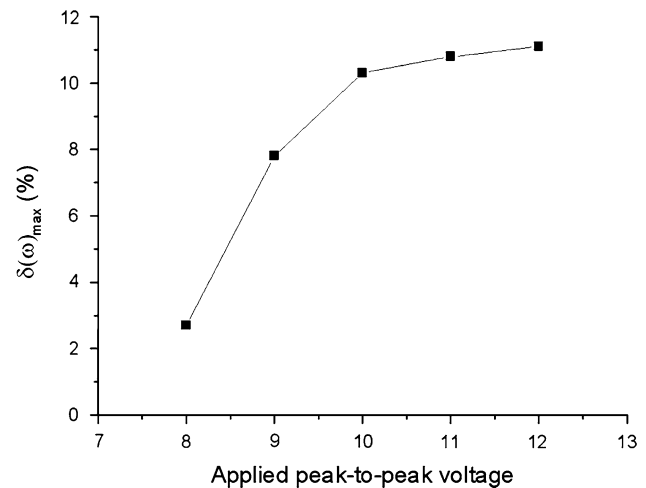


Fig. 12 Control effect with steady actuation of different applied voltages ($v_\infty = 50$ m/s, $i = 0^\circ$, $F = 23$ kHz, 70% Span)

the result in separation control of low-pressure turbine blades (Huang et al. 2006). Furthermore, higher voltage may lead to earlier destruction of the dielectric material, which is not desirable in the experiments.

3.2.3 Effect of the Reynolds number

When the freestream velocity decreases to 30 m/s (corresponding Re is 133,800), better control effect is obtained at the same applied peak-to-peak voltage, compared to that at 50 m/s, as shown in Figure 13. $\delta(\omega)_{\max}$ is 19.8%, when the applied peak-to-peak voltage and driving frequency are $V_{p-p} = 10$ kV and $F = 23$ kHz, respectively. When the freestream velocity increases to 70 m/s (corresponding Re is 312,200), almost no control effect is obtained, as shown in Fig. 14. Even when the applied peak-to-peak voltage

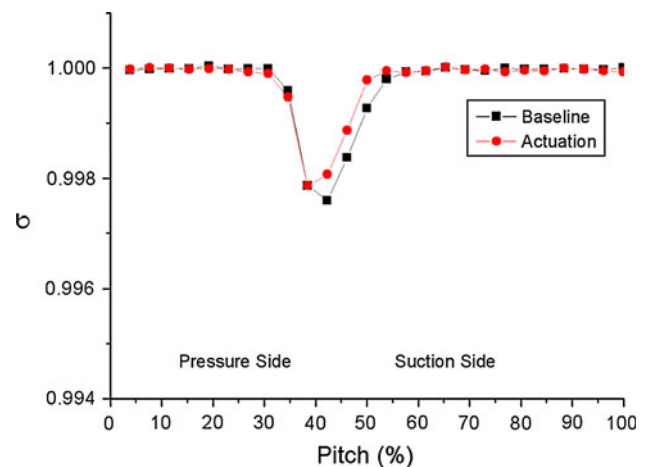


Fig. 13 Total pressure recovery coefficient distributions with and without steady plasma aerodynamic actuation at 70% blade span ($v_\infty = 30$ m/s, $i = 0^\circ$, $V_{p-p} = 10$ kV, $F = 23$ kHz)

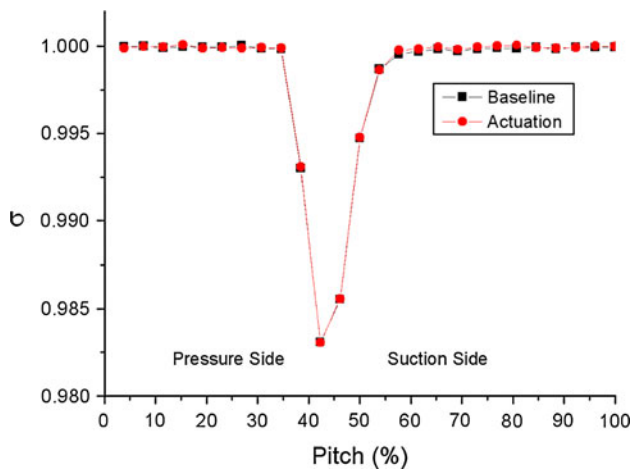


Fig. 14 Total pressure recovery coefficient distributions with and without steady plasma aerodynamic actuation at 70% blade span ($v_\infty = 70$ m/s, $i = 0^\circ$, $V_{p-p} = 10$ kV, $F = 23$ kHz)

increases to 12 kV, there is also no control effect. Therefore, along with the Reynolds number (freestream velocity) increasing, corner separation is more difficult to control, which is similar in airfoil leading edge flow separation control.

3.2.4 Effect of the angle of attack

When the angle of attack increases to 2° , total pressure recovery coefficient distributions along the pitch direction with and without steady plasma aerodynamic actuation at 70% blade span are shown in Fig. 15. All four electrode pairs are switched on. The applied peak-to-peak voltage and driving frequency are $V_{p-p} = 10$ kV and $F = 23$ kHz, respectively. $\delta(\omega)_{max}$ is 8.3%, which is less than that at 0° . When the angle of attack increases to 4° , $\delta(\omega)_{max}$ decreases to just 3.1%. The main reason for this phenomenon may be that the corner separation is more serious at higher angle of attack and more difficult to control.

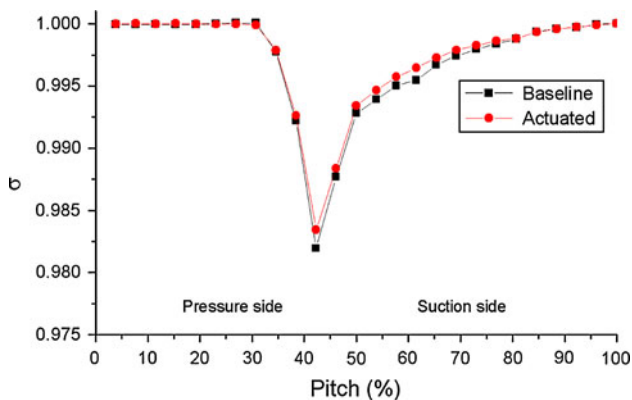


Fig. 15 Total pressure recovery coefficient distributions with and without steady plasma aerodynamic actuation at 70% blade span ($v_\infty = 50$ m/s, $i = 2^\circ$, $V_{p-p} = 10$ kV, $F = 23$ kHz)

3.3 Unsteady plasma flow control experiment results

Optimization of the excitation mode based on coupling between the plasma aerodynamic actuation and the separated flow is one of the important ways of improving plasma flow control effect. It has been shown in the literature that the introduction of unsteady disturbances near the separation location can cause the generation of large coherent vortical structures that could prevent or delay the onset of flow separation. These structures are thought to intermittently bring high momentum fluid to the surface, enabling the flow to withstand the adverse pressure gradient without separation. Periodic excitation by oscillatory blowing for separation control has been documented extensively (Greenblatt and Wygnanski 2000). Unsteady plasma aerodynamic actuation for separation control of low-pressure turbine blade (Huang et al. 2006) and airfoil (Corke et al. 2006; Benard et al. 2009) has been investigated.

3.3.1 Effect of the excitation frequency

A sensitive study is performed to determine whether such an optimum frequency exists for the unsteady actuation used in controlling the corner separation. Figure 16 documents the relative reductions in maximum total pressure loss coefficient at 70% blade span for a range of excitation frequencies from 100 to 1,000 Hz when the duty cycle is fixed at 60%. All four electrode pairs are switched on. The applied peak-to-peak voltage and driving frequency are $V_{p-p} = 10$ kV and $F = 23$ kHz, respectively.

When the excitation is 100 Hz, $\delta(\omega)_{max}$ is just 11.2%, which is almost as same as the steady control effect that is 10.7%. Along with the excitation frequency increasing, the

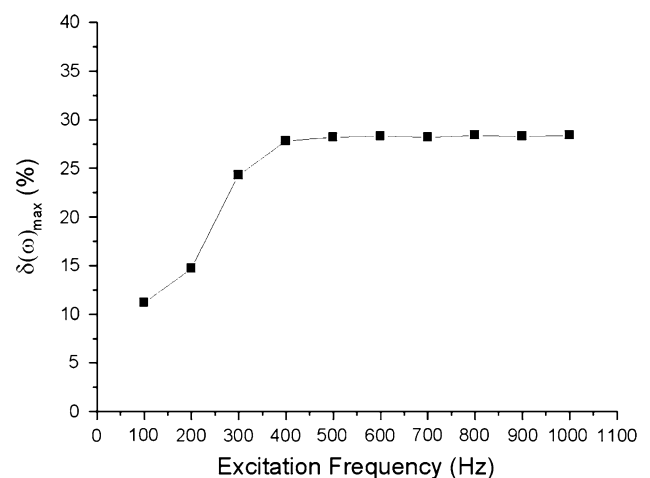


Fig. 16 Maximum relative reductions in total pressure loss coefficient with unsteady actuation of different duty cycles ($v_\infty = 50$ m/s, $i = 0^\circ$, $V_{p-p} = 10$ kV, $F = 23$ kHz, 70% Span)

control effect increases. When the excitation frequency is 400 Hz, $\delta(\omega)_{\max}$ increases to 28%. Thus, compared with the steady actuation, the unsteady actuation is much more effective and requires less power. When the excitation frequency is higher than 400 Hz, the control effect saturates, and further increases in the excitation frequency show no evident benefit. The difference between steady and unsteady plasma aerodynamic actuation may be that the unsteady pulsed operation allows the continuously generation of vortical structures, while the steady operation cannot. Vortical structures in the flow field promote momentum transfer in the boundary layer in order to withstand separation. Under different duty cycles and excitation frequencies, the coupling between actuation and flow field leads to different flow control effects.

Each electrode pair is switched onto study the effect of the actuation location. The control effect of all four electrode pairs is almost as same as that obtained by the 2nd electrode pair. The saturation frequency is also 400 Hz. For the 2nd electrode pair, the characteristic length is the remaining chord length downstream of the actuator, which is 75% chord length. Thus, the Strouhal number $Sr = f \times C/v_\infty$ is 0.4 when the frequency and freestream velocity are $f = 400$ Hz and $v_\infty = 50$ m/s, respectively. When the Strouhal number exceeds 0.4, the control effect saturates in the unsteady plasma flow control experiments. In the separation control above a NACA 0015 airfoil with unsteady plasma aerodynamic actuation (Benard et al. 2009), the most effective actuation was performed with a Strouhal number of Sr ranging from 0.2 to 1. In the separation control of low-pressure turbine blades with unsteady plasma aerodynamic actuation (Huang et al. 2006), the optimum excitation frequency is the one that makes the Strouhal number unity. Therefore, the optimum excitation frequency depends much on the flow separation state. Under different flow conditions, the optimum excitation frequency is also different.

3.3.2 Effect of the duty cycle

Figure 17 documents the maximum relative reductions in total pressure loss coefficient for a range of unsteady duty cycles from 5 to 100% when the excitation frequency is fixed at 400 Hz. All four electrode pairs are switched on. The applied peak-to-peak voltage and driving frequency are $V_{p-p} = 10$ kV and $F = 23$ kHz, respectively.

It is found that there is also a duty cycle threshold in controlling the corner separation. When the duty cycle is less than 60%, the control effect increases along with the duty cycle increasing. $\delta(\omega)_{\max}$ is 28% at the duty cycle of 60%. Even when the duty cycle is 5%, $\delta(\omega)_{\max}$ is 15.7%, much more effective than the steady actuation. When the duty cycle is higher than 60%, the control effect saturates

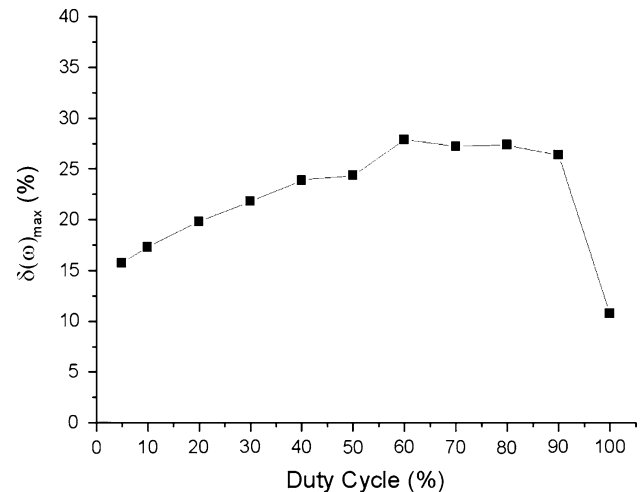


Fig. 17 Maximum relative reductions in total pressure loss coefficient with unsteady actuation of different duty cycles ($v_\infty = 50$ m/s, $i = 0^\circ$, $V_{p-p} = 10$ kV, $F = 23$ kHz, 70% Span)

along with the duty cycle increasing. Thus, it can be inferred that when the duty cycle is less than 60%, the injected energy is not sufficient to control the corner separation. In the separation control above a NACA 0015 airfoil with unsteady plasma aerodynamic actuation (Benard et al. 2009), the most effective duty cycle values range from 10 to 60%. In the separation control of low-pressure turbine blades with unsteady plasma aerodynamic actuation (Huang et al. 2006), the lowest plasma duty cycle (10%) was as effective as the highest plasma duty cycle (50%) at the same excitation frequency. Thus, the optimum duty cycle also depends much on the flow separation state.

4 Conclusions

Experimental results indicate that in the test cascade, the corner separation causes significant total pressure loss even when the angle of attack is 0° . Both steady plasma aerodynamic actuation and unsteady actuation are found to be effective in corner separation control when the freestream velocity and angle of attack are $v_\infty = 50$ m/s (corresponding Re is 223,000) and $i = 0^\circ$, respectively. For the steady plasma aerodynamic actuation, $\delta(\omega)_{\max}$ at 60 and 70% blade span are 13.8 and 10.7%, respectively. The control effect obtained by the electrode pair at 25% chord length is almost as same as that obtained by all four electrode pairs. The control effect obtained by the electrode pair at 5% chord length or 50% chord length are much less, while the electrode pair at 75% chord length contributes nothing to the control effect. Increase in the actuation voltage leads to better control effect, while the power dissipation increases from 8.4 to 23.5 W when the applied peak-to-peak voltage increases from 8 to 12 kV. When the

applied voltage is higher than 10 kV, the control effect saturates and further increases in the voltage amplitude show no evident benefit. Increasing the angle of attack or the freestream velocity makes the corner separation more difficult to control. Better control effect is obtained at 30 m/s, while there is no control effect at 70 m/s. The unsteady plasma aerodynamic actuation is more effective and requires less power. Maximum relative reduction in total pressure loss coefficient of 28% at 70% blade span was achieved when the duty cycle and excitation frequency are $\alpha = 60\%$ and $f = 400$ Hz, respectively. The obvious difference between steady and unsteady actuation may be that wall jet governs the flow control effect of steady actuation, while much more vortex induced by unsteady actuation is the reason for better control effect. There exists an excitation frequency threshold, which is 400 Hz in the experiments. The Strouhal number based on the characteristic length and the local freestream velocity is 0.4. The control effect shows saturation when the excitation frequency is higher than 400 Hz. There is also a threshold in the duty cycle, which is 60% in this paper.

Acknowledgments The authors thank Min JIA and Cheng-qin LI for the help in the experiment. This work was supported by the National Natural Science Foundation of China (50906100), China Postdoctoral Science Foundation (20090450373).

References

- Benard N, Braud P, Jolibois J, Moreau E (2008) Airflow reattachment along a NACA 0015 airfoil by surfaces dielectric barrier discharge actuator—time resolved particle image velocimetry investigation. In: AIAA paper 2008-4202. 4th Flow control conference. Seattle
- Benard N, Jolibois J, Moreau E (2009) Lift and drag performances of an axisymmetric airfoil controlled by plasma actuator. *J Electrostat* 67:133–139
- Boeuf JP, Lagmich Y, Unfer T, Callegari T, Pitchford LC (2007) Electrohydrodynamic force in dielectric barrier discharge plasma actuators. *J Phys D Appl Phys* 40:652–662
- Borcía G, Anderson C, Brown N (2003) Dielectric barrier discharge for surface treatment: application to selected polymers in film and fibre form. *Plasma Sources Sci Technol* 12:335–344
- Corke TC, Mertz B, Patel MP (2006) Plasma flow control optimized airfoil. In: AIAA Paper 2006-1208. 44th AIAA aerospace sciences meeting and exhibit. Reno
- Corke TC, Post ML, Orlov DM (2007) SDBD plasma enhanced aerodynamics: concepts, optimization and applications. *Prog Aerosp Sci* 43:193–217
- Dong Y, Gallimore SJ, Hodson HP (1987) Three-dimensional flows and loss reduction in axial compressors. *ASME J Turbomach* 109(3):354–361
- Falkenstein Z, Coogan J (1997) Microdischarge behaviour in the silent discharge of nitrogen oxygen and water air mixtures. *Appl Phys* 30:817–825
- Forte M, Jolibois J, Pons J, Moreau E, Touchard G, Cazalens M (2007) Optimization of a dielectric barrier discharge actuator by stationary and non-stationary measurements of the induced flow velocity: application to airflow control. *Exp Fluids* 42:917–928
- Gbadebo SA (2003) Three-dimensional separations in compressors. PhD thesis, University of Cambridge
- Gbadebo SA, Cumpsty NA, Hynes TP (2005) Three-dimensional separations in axial compressors. *ASME J Turbomach* 127(2):331–339
- Gbadebo SA, Cumpsty NA, Hynes TP (2008) Control of three-dimensional separations in axial compressors by tailored boundary layer suction. *ASME J Turbomach* 130(1):011004
- Greenblatt D, Wygnanski I (2000) The control of separation by period excitation. *Prog Aerosp Sci* 36:487–545
- Grundmann S, Tropea C (2007) Experimental transition delay using glow-discharge plasma actuators. *Exp Fluids* 42:653–657
- Hergt A, Meyer R, Engel K (2006) Experimental investigation of flow control in compressor cascades. In: ASME Paper GT2006-90415. ASME Turbo Expo 2006: Power for land, sea and air. Barcelona
- Huang J, Corke TC, Thomas FO (2006a) Plasma actuators for separation control of low-pressure turbine blades. *AIAA J* 44(1):51–57
- Huang J, Corke TC, Thomas FO (2006b) Unsteady plasma actuators for separation control of low-pressure turbine blades. *AIAA J* 44(7):1477–1487
- Jolibois J, Forte M, Moreau E (2008) Application of an AC barrier discharge actuator to control airflow separation above a NACA 0015 airfoil: optimization of the actuation location along the chord. *J Electrostat* 66:496–503
- Moreau E (2007) Airflow control by non-thermal plasma actuators. *J Phys D Appl Phys* 40:605–636
- Nersisyan G, Graham W (2004) Characterization of a dielectric barrier discharge operating in an open reactor with flowing helium. *Plasma Sources Sci Technol* 13:582–587
- Place JMM (1997) Three-dimensional flow in axial compressors. PhD thesis, University of Cambridge
- Roth JR, Sherman DM (2000) Electrohydrodynamic flow control with a glow-discharge surface plasma. *AIAA J* 38(7):1166–1172
- Samimy M, Kim J, Kastner J, Adamovich I, Utkin Y (2007) Active control of high-speed and high Reynolds number jets using plasma actuators. *J Fluid Mech* 578:305–330
- Sung Y, Kim W, Mungal MG, Cappelli MA (2006) Aerodynamic modification of flow over bluff objects by plasma actuation. *Exp Fluids* 41:479–486
- Wu Y, Li YH, Zhu JQ, Su CB, Liang H, Li G (2007) Experimental investigation of a subsonic compressor with plasma actuation treated casing. In: AIAA paper 2007-3849. 37th AIAA fluid dynamics conference and exhibit. Miami